

Linear bolometer array using a high TCR VO_x-Au film

Evan M. Smith^{1,2}, James C. Ginn¹, Andrew P. Warren¹, Christopher J. Long¹, Deep Panjwani²
Robert E. Peale², David J. Shelton¹

¹Plasmonics, Inc., 12605 Challenge Pkwy STE 150, Orlando FL 32826

²Department of Physics, University of Central Florida, Orlando FL 32816

ABSTRACT

We present a design for a low-noise bolometer linear array based on the temperature-dependent conductivity of a VO_x-Au film. Typical thin film bolometers must compromise between low resistivity to limit Johnson noise and high temperature coefficient of resistivity (TCR) to maximize responsivity. Our vanadium oxide is alloyed with a small concentration of gold by co-sputtering, which gives very low resistivity and very high TCR simultaneously. The film is fabricated on an air bridge device having high thermal conductivity and small thermal time constant optimized for 30 to 60 Hz frame rates. The linear array functions as a low-power profile sensor with a modulated bias. For 1 V bias, we predict responsivity exceeding 1200 V/W. Johnson noise dominates with predicted NEP values as low as 1.0×10^{-11} W/Hz^{1/2}. Preliminary device testing shows film resistivity below 2.5 Ω-cm with TCR exceeding -2.0%. Preliminary measurements of NEP and D* are reported.

Keywords: MEMS, bolometer, vanadium oxide, TCR

1. BACKGROUND

Vanadium oxide (VO_x) thin film for infrared detectors has been widely investigated^{1,2}. This semiconductor features a fairly low resistivity yet a high temperature coefficient of resistivity (TCR). Single crystal films of VO₂ can exhibit high TCR, but will generally have a semiconductor-to-metal transition temperature region where resistivity will change by orders of magnitude³. For VO₂ this occurs around 68°C. Amorphous vanadium oxide film, in contrast, has a much more stable TCR over a wide range of temperatures, which makes it a better candidate for thermal imaging applications.

Pure metal films typically increase their resistance, and insulators decrease theirs, as they heat up⁴. Insulators can have a high TCR, but their high resistance would equate to high Johnson noise, making thermal imaging impossible. A metal film will have low resistance, making it favorable from a Johnson noise perspective, but its TCR would be unacceptable low. Semiconducting VO_x exists in the realm between these states. Our hypothesis is that metal-doping would lower resistance without sacrificing TCR⁵. Gold was chosen as the dopant for its low resistivity and resistance to oxidation during deposition in oxygen plasma.

2. DESIGN

Gold-doped VO_x film (VO_x-Au) optimizes both the resistivity and TCR, where

$$TCR \equiv \alpha = \frac{1}{R} \frac{dR}{dT} . \quad (1)$$

An air-bridge design, with two nichrome arms on either side of the VO_x-Au film, achieves the thermal isolation needed for high response to incident power. The film is sandwiched between two layers of silicon dioxide to protect the VO_x-Au film during dry etching steps. The bridge sits above a gold reflector on the substrate surface to create a quarter-wavelength resonant cavity optimized for 10 μm absorption.

A current pulse is applied through the nichrome arms and across the VO_x-Au film while the voltage across the device is monitored. Incident infrared power causes heating, which changes the resistivity of the film according to

$$R = R_0(1 + \alpha dT), \quad (2)$$

where R_0 is the room-temperature resistance dT is the temperature increase of the film. Thus, a measure of incident power may be derived from a change in voltage across the device.

2.1 Responsivity

We consider the change in temperature of the device as a function of the incident power P_i . This is described by the heat flow equation

$$C \frac{\partial(\Delta T)}{\partial t} + G\Delta T = \eta P_i, \quad (3)$$

where η is the absorptivity, G is the total thermal conduction to the room-temperature surroundings and C is the heat capacity⁶. We assume that P_i is modulated with time dependence $e^{i\omega t}$ (fundamental of chopped signal used in testing) so that we seek a solution of the form $\Delta T e^{i\omega t}$. Using these assumptions, we solve Eq. 3 as

$$\Delta T = \kappa \frac{\eta P_i}{G}, \quad (4)$$

where κ is a coefficient related to the modulation frequency. The value of κ is close to unity for slow modulations. The heat capacity C affects the thermal time constant $\tau = \frac{C}{G}$. For a fixed input power, the change in temperature of the device is determined by absorptivity and heat loss via conduction. Ideal devices minimize heat loss by using long, thin isolation arms made of material with low conductivity.

The TCR of amorphous VO_x -Au is temperature-independent over a wide range of temperatures. Then by integrating Eq. 1, we obtain a linear relationship between the temperature change of the film and the natural logarithm of its resistance. The slope of that line is the TCR.

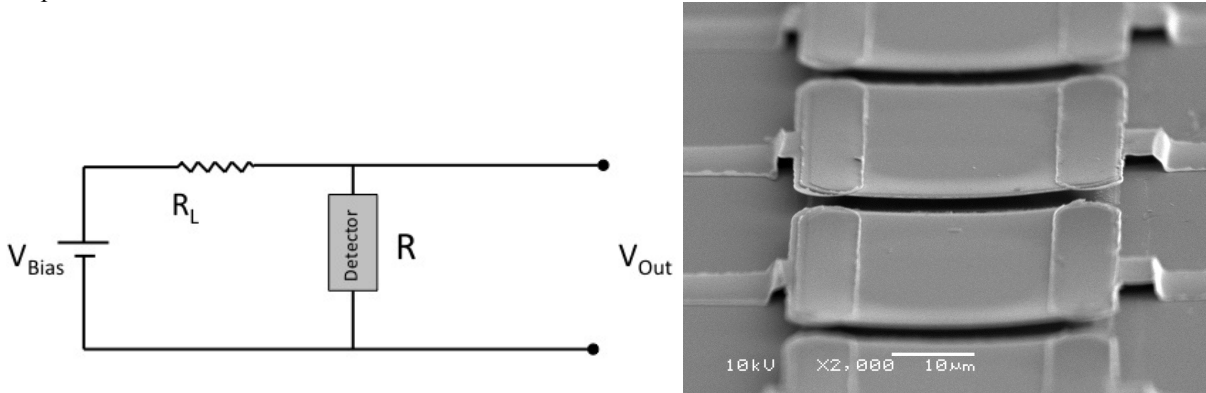


Figure 1: (left) Basic schematic for use of the detector. This circuit is not optimized for noise or detectivity. (right) SEM image of pixels from an array.

The sensitivity of a bolometer can be measured using the simple voltage divider circuit, shown in Fig. 1 (left). A bias voltage is applied across a load resistor and the detector. The detector is heated by both absorbed IR and Joule dissipation at rate i^2R . The output voltage is given by the voltage divider formula

$$V_{out} = V_B \frac{R}{R_L + R}. \quad (5)$$

The resistance of the bolometer determined from Eqs. 2 and 4 gives the differential output voltage, dV_{out} . If the load resistor is impedance-matched to the bolometer, then this differential voltage becomes⁶

$$dV_{out} = \kappa \frac{V_B \alpha \eta P_i}{4G_{eff}}. \quad (6)$$

where V_B is the bias voltage and G_{eff} is the effective thermal conduction considering impedance matching and joule heating. The $1/4$ term comes from the circuit design, where the output voltage is measuring only half of the circuit, and only the resistance of the device is changing. The voltage responsivity, R_v , is defined as the change in measured voltage as a function of incident power. Hence, we have

$$R_v = \frac{V_B \alpha \eta}{4G_{eff}} \frac{1}{\sqrt{1 + \omega^2 \tau^2}} \quad (7)$$

2.2 Noise

System noise has contributions from photon flux, the detector, and the electronic read-out. Generally, the largest and most easily adjusted contribution is from the detector itself. The bolometer is subject to Johnson noise, thermal fluctuation noise, and $1/f$ noise. Johnson noise is a variation in electrical resistance due to the temperature-dependent statistical fluctuations of charge carriers in the VO_x -Au film. Temperature fluctuation noise arises from the thermal non-equilibrium state of the detector in which thermal energy is constantly being exchanged with the environment. The $1/f$ noise is minimized by choosing sufficiently high modulation frequency.

The variance in voltage fluctuations due to Johnson noise is⁶

$$\delta V_j = \sqrt{4k_B T R \Delta f} \quad (8)$$

where Δf is the noise equivalent bandwidth, related to the integration time or modulation frequency. Temperature varies only slightly, so this noise voltage depends mainly on resistance. The signal-to-noise ratio (SNR) for Johnson noise is the found from the maximum signal voltage, Eq. 6, divided by the Johnson noise in Eq. 8. This ratio gives

$$SNR_j = \frac{V_B \alpha \eta P_i}{8G_{eff} \sqrt{k_B T R \Delta f}} \frac{1}{\sqrt{1 + \omega^2 \tau^2}} \quad (9)$$

Excessive bias voltage overheats the device, raises G_{eff} , and reduces SNR. Increased absorptivity η increases SNR, as does better thermal isolation. However, in terms of the active film, the best SNR comes from maximizing TCR α and minimizing resistance.

The RMS temperature fluctuation on the detector, derived from the heat-balance equation⁶, is

$$\sqrt{\Delta T^2} = \frac{2T \sqrt{Gk \Delta f}}{G \sqrt{1 + \omega^2 \tau^2}} \quad (10)$$

where ω is the modulation frequency as above. This temperature fluctuation causes a fluctuation in the film resistance, and hence a fluctuation in measured voltage. The SNR for thermal fluctuation noise can be found as a ratio of the absolute temperature of the bolometer, Eq. 4, to the temperature fluctuations, Eq. 10, and is

$$SNR_{TF} = \frac{\eta P_i}{2T \sqrt{Gk_B \Delta f}} \quad (11)$$

Decreasing the thermal conductance by providing better thermal isolation yields a better signal to noise ratio.

The Noise Equivalent Power (NEP) is

$$NEP = \frac{P_i}{SNR \sqrt{\Delta f}} \quad (12)$$

where NEP has units of Watts per root Hertz. For each noise contribution we find

$$NEP_j = \frac{8G_{eff} \sqrt{k_B T R} \sqrt{1 + \omega^2 \tau^2}}{V_B \alpha \eta} \quad (13)$$

$$NEP_{TF} = \frac{2T \sqrt{Gk_B}}{\eta} \quad (14)$$

The total detector noise is

$$NEP_T = \sqrt{(NEP_j)^2 + (NEP_{TF})^2} . \quad (15)$$

From the total NEP, the device D^* can be calculated as⁶

$$D^* = \frac{\sqrt{A}\sqrt{\Delta f}}{NEP} , \quad (16)$$

where A is the device active area, and Δf is the noise equivalent bandwidth, related to device integration time and clocking speed.

2.3 Numerical Calculations

We consider a device as shown in Figure 1 (right). The active area is the VO_x -Au film, which has an area of $35 \times 35 \mu m^2$. This is sandwiched between two layers of silicon dioxide and suspended above a reflecting gold pad to make a resonant cavity optimized for 8-12 μm absorption. Thin NiCr arms on either side provide support for the structure as well as electrical conductivity. SiO_2 has a heat capacity of 0.7 J/gK with a density of 2.2 g/cm³. There is currently no data specifically for the VO_x -Au film that we are developing, so properties of VO_2 are used in its place, which has a heat capacity of 0.3 J/gK and a density of 3.36 g/cm³.

The heat capacity of the device is given by

$$C_i = c_i \rho_i t_i A , \quad (17)$$

where c is the material heat capacity, ρ is the density, t is the thickness, A is the area, and the subscript i denotes the layer. The total heat capacity then is the sum of the heat capacity for each SiO_2 layer and for the VO_x -Au film. Using the parameters given, the heat capacity is 5×10^{-10} J/K.

The thermal conductance of the bolometer is

$$G = 2 \frac{g_{NiCr} t w}{l} + 4\epsilon\sigma AT^3 , \quad (18)$$

where the first term is the conductance through the two arms of the device, where g is the thermal conductivity of NiCr of 11.3 W/mK. The second term is conductance by radiation. This assumes that the device is held in vacuum, and there is no thermal conduction by air molecules. By Eq. 18, we find the thermal conductance through the arms is 2.7×10^{-6} W/K, and the thermal conductance by radiation is 3×10^{-8} W/K near room temperature. From the heat capacity and thermal conductance, we find the thermal time constant to be $\tau = 184 \mu s$.

We solve Eq. 4 for a 100 nW incident power and assuming a 64% absorptivity based upon simulations for a Fabry-Perot cavity in a range of 8-14 μm . Using the thermal conductance of 2.7×10^{-6} W/K, the temperature of the device will rise by $\Delta T_d = 23.7$ mK. We have measured the sheet resistance of VO_x -Au films at room temperature to be about 250 k Ω with a TCR of about -2.0%. For the given temperature change, this would give a resistance change of about 474 m Ω .

The responsivity of the device is found from Eq. 7. From values already determined, using a bias voltage of 1.0 V, we predict a voltage responsivity of 1184 V/W. By Eqns. 13-15, we find the NEP for Johnson noise and thermal fluctuation noise to be 5.4×10^{-11} W and 5.7×10^{-12} W, respectively, resulting in a total NEP of 5.5×10^{-11} W.

3. FABRICATION

The air bridge structure is built on an oxidized silicon wafer for electrical isolation. Gold reflectors are patterned where the elements will eventually sit. The air bridge structure is achieved by first depositing a sacrificial polyimide and using a wet etch process to form it into pillars of the desired thickness and lateral dimension. The slope on the walls of this polyimide pillar is as shallow as 70° to as steep as 90° (Fig 2, left), with occasional undercutting. Structural considerations with the support arms favor shallow-sloped sidewalls. Thus, the polyimide is ashed in a Branson barrel asher using an O_2/CF_4 plasma, which yields sidewalls much closer to 45° (Fig 2, right).

Now the element is patterned on the polyimide. Because the active film VO_x -Au etches quickly in any plasma, the film is sandwiched in between two layers of silicon dioxide. Low-stress nichrome (80/20 nickel/chrome) arms are sputtered

in argon plasma at high pressure. These arms provide structural stability and electrical continuity. They stretch over the polyimide pillar, so that the slope of the polyimide sidewalls corresponds to the slope of these arms.

The final step in the process is the removal of the cured polyimide to create a free-standing air bridge with two nichrome anchors. The sample is placed in the same barrel asher as used before but now etched only in an oxygen plasma.

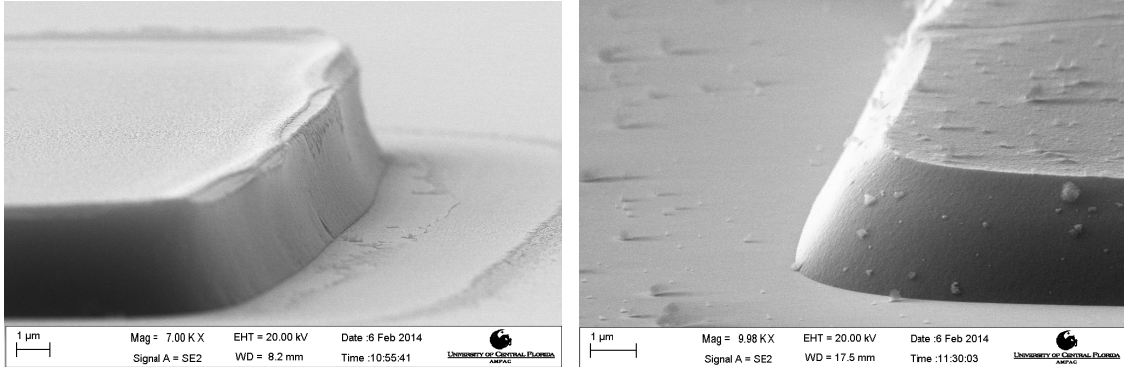


Fig 2 (Left) Polyimide sidewalls before ashing. Slope is above 75°. (Right) Polyimide sidewall after ashing. The slope is much more shallow here.

3.1 VO_x-Au Development

The VO_x-Au films were deposited using a reactive DC magnetron sputtering process that co-sputters vanadium and gold in an oxygen-rich plasma. Chamber pressure and gas concentration are controlled. The substrate surface energy can be changed by RF biasing. Concentrations of oxygen, vanadium, and gold are thus optimized so that pure vanadium was oxidized en route to the substrate to form VO_x. The gold is co-sputtered at a low rate to keep the concentration small.

Fig. 3 presents a plot of resistivity vs TCR for differently prepared films. Gold was deposited at 0, 10, and 20 W giving rates of approximately 0, 10 and 20 Å/min, respectively. Oxygen concentration was 20 or 30%, while chamber pressure was 4 or 10 mTorr. Finally, the substrates were either unbiased or RF biased at 40 W (~240 V applied). The relationship between the TCR and log resistivity is linear. Superior films fall under the line. Pure VO_x film has the most negative TCR. A small addition of gold significantly drops the resistivity. Introducing a negative plasma potential by RF biasing is shown to consistently lower the resistivity for a given TCR. This changes the density of the film and removes impurities.

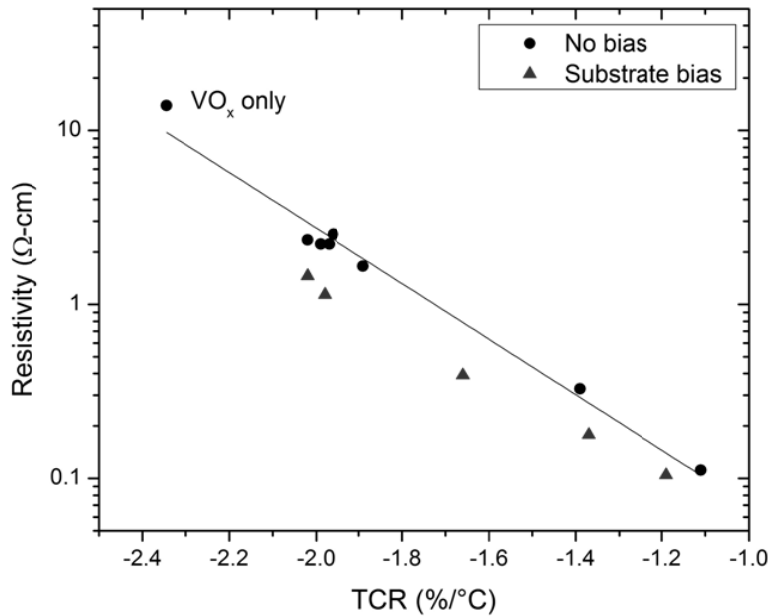


Fig. 3. TCR vs. room temperature resistivity for a number of different deposition parameters. The addition of an RF bias reduces the resistivity while not changing TCR.

The optimum sputtering condition uses four vanadium targets all set at 200W, and one gold target set at 10 W, in a nominal oxygen concentration of 20%, at 4 mTorr chamber pressure. Without RF bias, resistivity of this film averages around 2.3 Ω-cm with a TCR of -1.99%; 40 W RF substrate bias drops the resistivity down to about 1.3 Ω-cm without changing the TCR. For a film of 110 nm thickness (as measured by a stylus profilometer) this gives a sheet resistance of about 210 kΩ/□ and 120 kΩ/□ for conditions without and with RF bias, respectively.

Subsequent films were made on carbon substrates and analyzed by Rutherford Backscattering technique to determine a film composition of approximately 33.5% molar vanadium, 62.5% molar oxygen, and 4% molar gold, for which the amorphous vanadium oxide is VO_{1.87} with less than 10% uncertainty.

4. DEVICE TESTING

Figure 4 (left) shows the design schematic for testing both the responsivity and the noise of the device. A blackbody source (IR-301 Infrared Systems Development Corporation) is used as the power source. An optical chopper modulates the signal. This chopper has a high emissivity on the front side (facing the detector) but a low emissivity facing the blackbody to limit heating. The detector is placed a distance $r = 14$ cm away from the blackbody source. It is housed in a vacuum-sealed container to provide better thermal isolation for the air bridge. The detector is DC biased and the output voltage is monitored on an oscilloscope and a lock-in amplifier referenced to the chopper. The signal on the detector is given by⁶

$$P_i(T) = \Delta L(T) \frac{A_{BB} A_d}{r^2} F_f \tau, \tag{19}$$

where A_{BB} is the area of the blackbody (26.4 cm²), A_d is the area of the detector, r is the distance between the blackbody and detector, τ is the transmission of the window of the detector housing, and F_f is the form factor to convert a peak-to-peak signal to RMS values. The window is a Thallium Bromo-Iodide window, which has a transmission of ~70% from 0.6-40 μm. The radiance term, ΔL , is determined by evaluating Plank's Law in the wavelength range of the window:

$$L = + \frac{2k^4 T^4}{h^3 c^2} \int_{x_2}^{x_1} \frac{x^3}{e^x - 1} dx, \quad x = \frac{hc}{\lambda kT}. \tag{20}$$

Solving Eq. 20 at room temperature between 0.6 and 40 μm gives a background radiance of 13.07 mW/cm² sr. At a blackbody temperature of 300°C, the radiance becomes 192.62 mW/cm² sr, giving a differential radiance of 179.55 mW/cm² sr. From Eq. 19, the power incident on a detector given the conditions described is 207.54 nW.

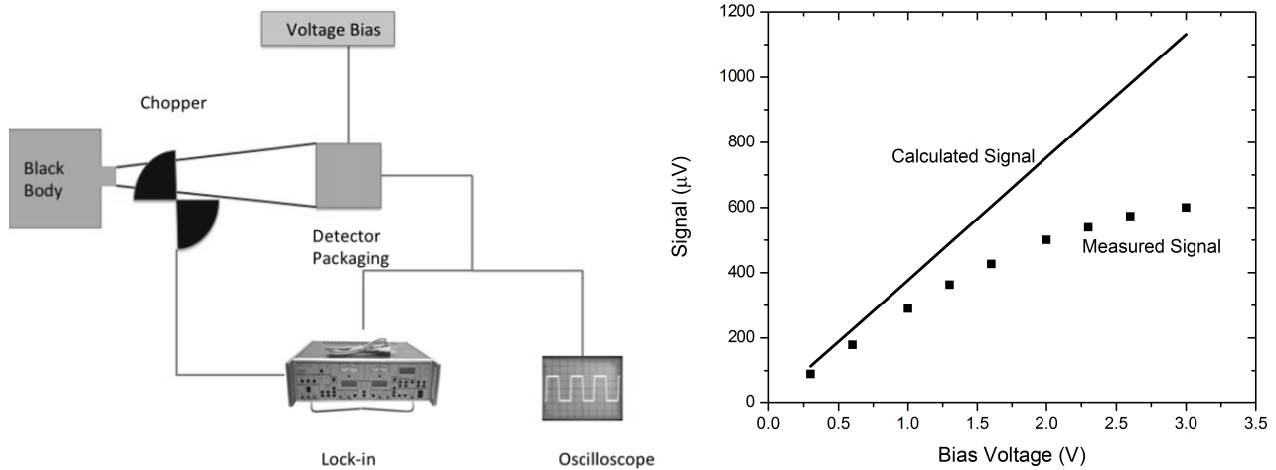


Fig 4. (left) Schematic of the device test configuration. (right) Bias voltage vs. signal voltage. The calculation neglects Joule heating.

A completed, functioning detector is placed into vacuum-sealed packaging and incident radiation from the blackbody falls on the active area while signal is determined. To measure noise, the blackbody is blocked by a highly emissive piece of metal held at room temperature. The signal measured in this configuration is the noise. Table 1 gives the results of tests on a single device. These tests are done with a blackbody at 500°C placed 14 cm from the detector, with a chopper modulating the signal at 87 Hz. The sample has a nominal resistance of 90.3 kΩ. The detector shows strong performance for integration times of both 1 and 30 milliseconds, although the latter generally has a higher signal to noise ratio. Signal increases with bias voltage as presented in Fig. 4 (right). Theory suggests a linear relationship, in contrast to the experimental data. This due to the Joule heating, which heats the film independent of absorbed IR.

Table 1. Performance characteristics of a single pixel on wafer ES019, with a blackbody at 500°C positioned 14 cm away from the detector. The incident power is 726 nW.

Bias Voltage [V]	Time Constant [msec]	Calculated Signal [μV]	Measured Signal [μV]	Measured Noise [μV]	SNR	NEP [10 ⁻¹⁰ W]	D* [x 10 ⁸ cm Hz ^{1/2} W ⁻¹]
0.3	1	113.5	89.6	0.05	1792	4.05	1.93
0.3	30	113.5	90.1	0.025	3604	2.01	0.71
0.6	1	226.2	179	0.055	3254	2.23	3.51
0.6	30	226.2	178	0.07	2543	2.85	0.51
1	1	377.1	290	0.1	2903	2.50	3.13
1	30	377.1	289	0.05	5774	1.26	1.14
1.3	1	490.2	363	0.125	2904	2.50	3.13
1.3	30	490.2	366	0.07	5235	1.39	1.03
1.6	1	603.4	427	0.11	3416	2.13	3.68
1.6	30	603.4	28	0.125	3895	1.86	0.77
2	1	754.1	501	0.15	3340	2.17	3.6
2	30	754.1	501	0.11	4554	1.59	0.89
2.3	1	867.2	539	0.17	3170	2.29	3.42
2.3	30	867.2	539	0.14	3850	1.89	0.76
2.6	1	980.3	573	0.16	3581	2.03	3.86
2.6	30	980.3	573	0.14	4092	1.77	0.81
3	1	1131.2	600	0.2	3000	2.42	3.23
3	30	1131.2	600	0.16	3750	1.94	0.74

The best D* values are in the range of 10⁸, which correspond to an NETD value of less than 100 mK. As the system is enhanced, we should be able to push the limits on performance without sacrificing the design or integration time.

5. GOLDBLACK ABSORBER

To achieve the higher absorption needed to improve detectivity, we consider an additional infrared absorbing layer. The layer must have low thermal mass and heat capacity to avoid slowing the response. Gold-black satisfies these conditions⁷. This paper presents the first practical application of a novel means of patterning this usually fragile deposit⁸. Standard photolithography and lift-off in acetone is enabled by an evaporated 200 nm thick SiO₂ protection layer⁸. Fig. 5 presents SEM images that demonstrate successful patterning and placement of gold-black absorbers directly on the air-bridges. Absorption is somewhat reduced in 8-12 μm range with respect to unprotected gold black, but it is still expected to exceed 75%⁸. Interestingly, the goldblack layer survived the dry etch in oxygen plasma of the air-bridges from the polyimide sacrificial layer. Future efforts will focus on characterizing the bolometer with goldblack over-coated pixels.

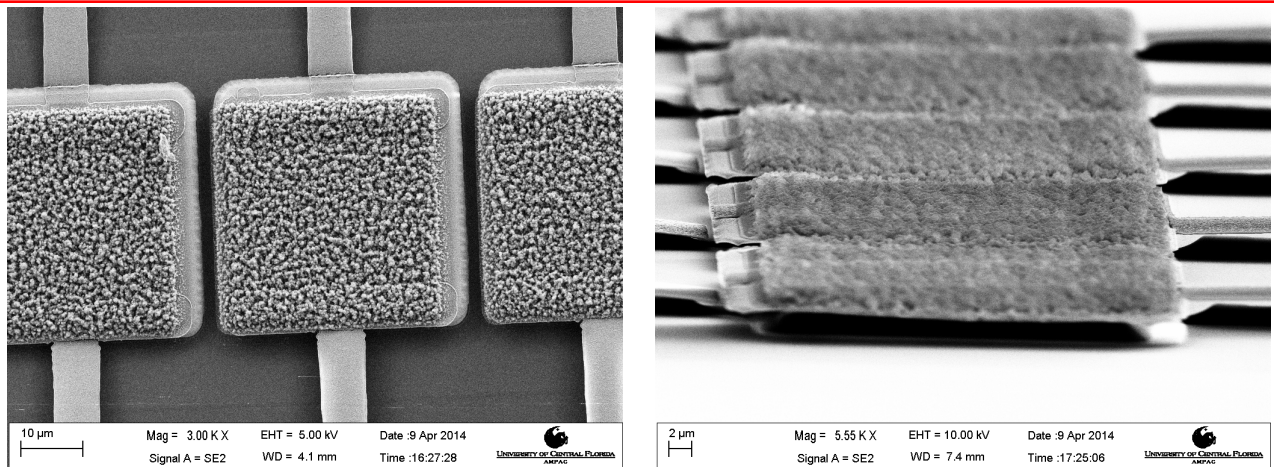


Fig. 5. SEM image showing top (left) view of pixels from an array coated with SiO_2 protected goldblack absorber. The cross-sectional (right) view shows freestanding pixel after dry etching of sacrificial layer.

6. CONCLUSION

We have developed a bolometer optimized for the 8-12 μm region based upon a novel VO_x -Au film that has a low resistivity without sacrificing TCR. Optimization of the film, the thermal conductance, and the absorptivity allows for a high signal-to-noise ratio, which results in a calculated NEP of 5.5×10^{-11} and measured best NEP of 2.13×10^{-10} W at a 1 millisecond integration time. The difference of an order of magnitude is mainly due to system noise, not necessarily to the detector itself. One simple change to improve the system quality would be to replace a load resistor with a dark bolometer that would heat and cool based on environmental and bias voltage effects, just as the active bolometer would. As such, the detector records a D^* of close to 4×10^{10} $\text{cm Hz}^{1/2}/\text{W}$, which gives an NETD of below 100 mK. Further optimization of the testing apparatus as well as introducing the goldblack absorbing layer will push the NETD even lower.

ACKNOWLEDGMENTS

This research was supported by a grant from the US Army Research Labs (ARL) SBIR program. We would also like to acknowledge the support and assistance from Mr. Guy Zummo, Mr. Ed Dein and Prof. Kevin Coffey.

REFERENCES

- [1] Chen, Tao, Hu, Ming, Liang, Ji-ran, Lu, Jia-ning, Tan, Lei, "Study on Preparation of Vanadium Oxide Thin Films by the Metal-oxygenation method," Proc. SPIE 7381, (2009)
- [2] Niklaus, Frank, Vieider, Christian, Jakobsen, Henrik, "MEMS-Based Uncooled Infrared Bolometer Arrays-A Review," Proc. SPIE 6836, (2007)
- [3] Morin, F.J. "Oxides Which Show a Metal-to-Insulator Transition at the Neel Temperature," Phys. Rev. Lett 3(1): 34-36, (1959)
- [4] Dunlap, R.A. [Experimental Physics], Oxford University Press, New York, (1988)
- [5] Lam, Vu H., [Electrical Properties of Reactive Magnetron Sputtered Vanadium Oxide Thin Films], Masters Thesis, UCF, Orlando, (2005).
- [6] Dereniak, E.L and Boreman, G.D. [Infrared Detectors and Systems], John Wiley and Sons, New York, (1996)
- [7] W. Becker, R. Fettig, W. Ruppel, "Optical and electrical properties of black gold layers in the far infrared", Infrared Physics & Technology 40: 431-445 (1999)
- [8] Deep Panjwani, Mehmet Yesiltas, Janardan Nath, D.E. Maukonen, Imen Rezadad, Evan M. Smith, R.E. Peale, Carol Hirschmugl, Julia Sedlmair, Ralf Wehlitz, Miriam Unger, Glenn Boreman, "Patterning of oxide-hardened gold black by photolithography and metal lift-off, Infrared Physics & Technology", 62: 94-99 (2014)